Modeling land-atmosphere energy and water exchanges in the typical alpine grassland in Tibetan Plateau using Noah-MP

Ning Ma

Key Laboratory of Water Cycle and Related Land Surface Processes, Institute of Geographic Sciences and Natural Resources Research, Chinese Academy of Sciences, Beijing, China

ABSTRACT

Study region: Alpine grassland in the Tibetan Plateau
Study focus: This study used Noah-MP to simulate the energy fluxes [net radiation (Rn), latent (λE) and sensible (H) heat fluxes] in two typical alpine ecosystems in the Tibetan Plateau. The effectivenesses of new parameterization schemes for the roughness length for heat transfer and the root distribution were evaluated. By further using multi-scenario modeling, the responses of land evapotranspiration (ET), soil evaporation (E_s) and vegetation transpiration (T_r) to changes in precipitation, solar radiation and air temperature were investigated.
New hydrological insights for the region: The default Noah-MP largely overestimates (underestimates) R_n and λE, but tends to underestimate (overestimate) H in alpine meadow (alpine steppe). After incorporating two newly-developed parameterization schemes, the accurancy of Noah-MP has been improved in alpine meadow for R_n and λE, while in alpine steppe only H has been improved. The ET, E_s and T_r in alpine meadow are more sensitive to decreasing precipitation than that to increasing precipitation. In alpine steppe, ET and E_s increase with increasing precipitation, while T_r responds weakly to changes in precipitation; The effect of temperature change on ET appears weak in both ecosystems. However, T_r shows negative responses to increased temperature and such responses in alpine steppe are more remarkable than those in alpine meadow, suggesting the former may be more vulnerable to future warming than the latter.

1. Introduction

As a key component of climate models, land surface models (LSMs) provide lower boundary conditions for climate models by simulating biophysical and biochemical processes (Bonan and Doney, 2018; Sellers et al., 1997). Typically, LSMs utilize complex mathematical methods to describe physical processes at the surface, requiring a larger number of parameters as inputs (Clark et al., 2015; Pitman, 2003). In large-scale applications, LSMs mostly describe the transport processes of mass and energy through the soil-vegetation-atmosphere firstly in the vertical direction at a one-dimensional grid, and then consider the influence of the topography in space by using digital elevation models (Clark et al., 2017; Niu and Zeng, 2012). Therefore, the assessment of LSMs at the plot scale is the first step to understand the skill of LSMs in simulating land surface processes over different land covers (Bonan et al., 2011; Fisher and Koven, 2020; Zhang et al., 2022).

The Tibetan Plateau (TP), known as the "the Third Pole of the World", is the highest and the largest plateau in the world. It has a mean elevation of approximately 4000 m and an area of approximately 2.65×10^6 km². As such, the thermal and dynamic effects of TP

play a vital role in determining the weather and climate in the Northen Hemisphere (Xie et al., 2023; Wu et al., 2015). In particular, the release of land surface sensible and latent heat from Tibetan Plateau has a remarkable influence on the atmospheric circulation and the regional climate (Huang et al., 2023). In the past decade, substantial advances in observations (Ma et al., 2023) and modeling (Lu et al., 2020) of the land surface processes in TP have been made by the community. In terms of the latter, after introducing new parameterization schemes for soil water flow, Yang et al. (2009a) found that the SiB2′s skill in simulating latent heat flux (λE) can be significantly improved. Li et al. (2014) evaluated SiB2 in an alpine meadow in the upper reach of the Heihe River Basin and they found that the model's accuracy in the surface conductance is particularly critical for λE simulation. In addition, numerous studies have dedicated into understanding of the role of roughness length on the land surface modeling. For example, the studies in the western TP by Chen et al. (2010) and northeastern TP by Zheng et al. (2014) evaluated the influence of different roughness length parameterization schemes on the soil temperature and moisture as well as turbulence fluxes simulated by Noah. Using ground observations of at the Maqu station in the source region of Yellow River, Zheng et al. (2015a), (2015b) took into account the effect of vegetation on soil heat transfer and modified the parameterization scheme of soil vertical physicochemical properties in Noah, largely improving the model's skill in simulating the land-atmosphere energy and water exchanges.

By improving the realism of Noah in a variety of representations of terrestrial biophysical and hydrological processes, the Noah LSM with multiparameterization options (Noah-MP) (Niu et al., 2011) was designed for a full spectrum of environmental conditions worldwide. Noah-MP has now been widely used by the atmospheric and hydrological communities for weather forecast and short-term climate predictions by coupling to the Weather Research and Forecast Model (Warrach-Sagi et al., 2022), for hydrological predictions by coupling to the National Water Model (Cosgrove et al., 2017), and for data assimilation by coupling to the National Center for Atmospheric Research High-Resolution Land Data Assimilation System (He et al., 2023). Previous model evaluations in the United States (Cai et al., 2014; Ma et al., 2017), China (Liang et al., 2019) and the whole globe (Li et al., 2022) have suggested that Noah-MP can well simulate the land-atmosphere energy, water and carbon exchanges at varying spatial scales. While there have also been a great number of studies in assessing Noah-MP in TP (e.g., Gao et al., 2015; Sun et al., 2022; Zheng et al., 2015c), most studies only focus on the alpine meadow in the eastern TP. However, the land surface is particularly heterogeneous in TP. Therefore, more evaluations in different land cover types remain needed to provide a holistic understanding of Noah-MP in such a high elevation region, as has also been advocated by Lu et al. (2020).

The alpine grassland, with an area accounting for ~55% of the total area of TP (Ma and Zhang, 2022a), is the dominant land cover type in TP (Miehe et al., 2011). The alpine grassland consists of two major ecosystem types, i.e., alpine steppe and alpine meadow (Fig. 1), with similar total area of 71.3×10^4 km^2 and 70.5×10^4 km^2, respectively. The primary differences between these two ecosystems are the climate and vegetation conditions. In general, the alpine steppe is mainly located in the western part of TP with an arid climate and its dominant species include *Stipa purpurea* and *Carex moorcroftii*, while alpine meadow is mainly distributed in the eastern part of TP with a relatively wet climate and its dominant species include *Kobresia pygmaea* and *Kobresia humilis* (Zhang et al., 1988). The ecosystem-averaged growing season-mean leaf area index (LAI) are 0.16 and 0.76 for alpine steppe and alpine meadow, respectively (Ma and Zhang, 2022a). By simultaneously focusing on these two alpine ecosystems, here we used Noah-MP to simulate the energy fluxes [i.e., net radiation (R_n), sensible (H) and latent heat fluxes (λE)] during summer. The objectives of this study are to (i) improve the parameterization schemes for the roughness length for heat transfer and the root distribution in Noah-MP to better simulate land-atmosphere energy and water exchanges in the alpine grassland of TP; and; (ii) evaluate the responses of land evapotranspiration (ET) and its components—soil evaporation (E_s) and plant transpiration (T_r)—to changing meteorological conditions, thus providing insights into the impacts of future climate change on the Tibetan alpine grassland.
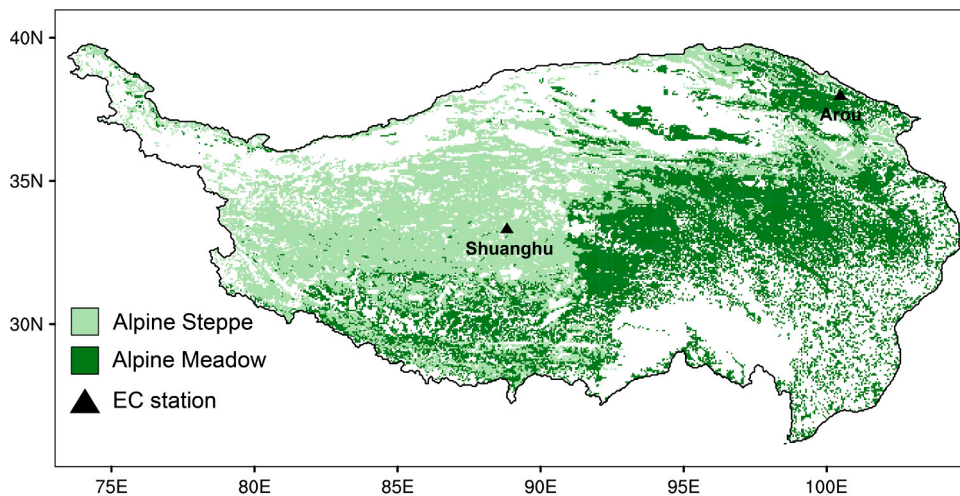

Fig. 1. Spatial distribution of alpine meadow and alpine steppe in the Tibetan Plateau and the geographical location of two eddy-covariance flux stations (Arou and Shuanghu).

2. Materials and methods

2.1. A brief description of Noah-MP

In the present study, the Noah-MP used is the version proposed by Niu et al. (2011). Noah-MP numerically describes the states of terrestrial energy, water, carbon and associated flux exchanges between the land surface and the atmosphere that are controlled by terrestrial hydrometeorological and ecohydrological processes (Niu et al., 2011). Based on Noah (Chen and Dudhia, 2001), Noah-MP was first augmented with vegetation and groundwater dynamics (Niu and Yang, 2007) and then equipped with multiple schemes for each of ecohydrological process (Niu et al., 2011). Noah-MP has a structure of one canopy layer, three snow layers, and four soil layers. It computes surface temperature by iteratively solving the surface energy balance of solar radiation, longwave radiation, sensible heat, latent heat, and ground heat fluxes. Noah-MP explicitly represents evaporation from the soil surface, canopy interception loss, and transpiration through formulations in analogy to the Ohm's law considering aerodynamic and stomatal resistances to the water vapor and carbon fluxes within and over the plant canopies. Plant transpiration is limited by the stomatal resistance, which is controlled by the root-zone soil moisture (Niu et al., 2011). Noah-MP assumes uniformly distributed roots in the vertical direction, but the root depth depends on vegetation types.

2.2. Modification of Noah-MP with improved parameterization schemes in TP

2.2.1. Roughness length for heat transfer

The roughness length for heat transfer (z_{oh}) and momentum (z_{om}) are two key parameters in determining the land-atmosphere energy exchanges. Typically, the z_{om} could easily be determined by either look-up table method or vegetation height. However, the z_{oh} in Noah-MP is determined by:

$$\frac{z_{0h}}{z_{0m}} = \exp(-k \quad C_{zil} \sqrt{Re_*}) \tag{1}$$

$$Re_* = \frac{U_* \quad z_{0m}}{v} \tag{2}$$

in which k is the von Karman constant ($= 0.4$), Re_* is the Reynolds roughness number, U_* is the friction velocity, v is the Molecular kinematic viscosity coefficient ($= 1.5 \times 10^{-5}$ m^2 s^{-1}), C_{zil} is a parameter that assumes to be 0.1 (Chen et al., 1997) in the default Noah-MP setting.

Note that the 0.1 for C_{zil} is a global universal value and may be not appropriate to TP. Using the eddy-covariance observations, Chen and Zhang (2009) found that there are substantial differences in across different ecosystem. Thus, a new scheme for C_{zil} is proposed using the vegetation height (h), i.e.,

$$C_{zil} = 10^{(-0.4h)} \tag{3}$$

Eq. (3) explicitly considers the impact of land cover conditions on the roughness length, which is more appropriate for different ecosystems. In this study, we would use the measured vegetation height in Eq. (3) to derive new C_{zil} that can provide more accurate estimation of z_{oh}.

2.2.2. Root distribution

The root water uptake primarily determines the plant transpiration (T_r). In Noah-MP, T_r is the accumulative value of transpiration from each root zone layer:

$$T_{r,i} = T_r * EFR_i \tag{4}$$

in which EFR_i is the ratio of effective root in the ith layer, $T_{r,i}$ is the transpiration contributed by the ith layer.

$$EFR_i = \frac{F_{sw,i} * F_{root,i}}{\beta_t} \tag{5}$$

where β_t is a soil water limiting factor that regulates the plant transpiration:

$$\beta_t = \sum_{i=1}^{nroot} F_{sw,i} * F_{root,i} \tag{6}$$

in which $F_{sw,i}$ is the available water for the ith soil layer, $F_{root,i}$ is the ratio of root in the ith layer to the total root, $nroot$ is the total number of root layer. Noah-MP provides three different parameterization schemes for $F_{sw,i}$ (Niu et al., 2011) and the present study mainly used the one based on Noah (Ek et al., 2003) (see Section 2.4). For the $F_{root,i}$, the default Noah-MP assumes that the root is homogeneous in each layer, i.e.,

$$F_{root,i} = \frac{\Delta d_i}{\sum_{i=1}^{nroot} \Delta d_i} \tag{7}$$

where the Δd_i is the thickness of the *i*th root layer.

However, our field observations of roots in alpine grassland found that the root are mainly distributed in upper layers, while in the lower layers the roots become much less. This suggests that the roots are heterogeneously distributed along the vertical direction in the alpine grassland. To make the model considers the real condition of TP, we employed the asymptotic nonlinear model proposed by Gale and Grigal (1987):

$$FR = 1 - X^{100*z} \tag{8}$$

in which the *FR* means the cumulative root fraction from the land surface to the depth of *z* (m), *X* is a parameter that needs to calibrated against observations, and 100 is used to transfer the unit of meter to centimeter. The large-sample field investigations in alpine grassland in the Tibetan Plateau by Yang et al. (2009b) suggest that *X* could be taken as 0.937 and 0.9 for alpine meadow and alpine steppe, respectively. Based on Eq. (8), one can rearrange the Eq. (7) to better represent the real conditions in Tibetan alpine grassland, i.e.,

$$F_{root,i} = \begin{cases} \dfrac{1 - X^{100*\Delta d_i}}{1 - X^{\sum\limits_{i=1}^{nroot} 100*\Delta d_i}}, i = 1 \\[4mm] \dfrac{1 - X^{\sum\limits_{j=1}^{i} 100*\Delta d_j}}{1 - X^{\sum\limits_{i=1}^{nroot} 100*\Delta d_i}} - F_{root,i-1}, 1 < i < nroot \end{cases} \tag{9}$$

In the present study, we would take Eq. (9) as the new root distribution scheme to test the impact of root distribution on the modeled energy fluxes in alpine meadow and alpine steppe.

2.3. Observations of land-atmosphere interactions in two typical stations

In this study, the observations from two eddy-covariance flux stations including Arou Station and Shuanghu Station (Fig. 1) are used to drive the Noah-MP in an off-line manner for the plot-scale energy fluxes simulations.

The Arou Station (Liu et al., 2018; Li et al., 2013) is located in a typical alpine meadow in the upper reach of the Heihe River Basin in the northeastern TP with an elevation of 3033 m. The observation site is overall flat with homogeneous vegetation coverage. The mean canopy height is ca. 20 cm and maximum LAI is ca. 5 during growing season. The soil belongs to silt loam and is usually frozen during October-May of ensuing year. The annual mean temperature is ca. 1 °C, with July of roughly 13 °C, down to ca. − 13 °C in January (Li et al., 2014). The annual precipitation is about 500–700 mm, of which 80% occurred during June to September. Details of the observation instruments in the Arou Station are provided by Liu et al. (2018).

The Shuanghu Station (Ma et al., 2015a, 2015b) is located in a typical alpine steppe in the central TP with an elevation of 4947 m. The Shuanghu Station has annual mean temperature of − 3.3 °C, with monthly averages of − 10.1 °C for January and 9.1 °C for July. The multiyear mean annual precipitation was ca. 330 mm, falling mainly between June and September. The observation site is homogenously flat with a fetch of > 1 km for the prevailing wind direction. The soil belongs to sandy loam. The mean canopy height during growing season is 0.03 m. The maximum LAI is about 1 and the maximum above-ground biomass is estimated as ca. 50 g m^{-2} in summer. Details of the observation instruments in the Shuang Station are provided by Ma et al. (2015a), (2015b).

2.4. Modeling protocol

To avoid the influence of soil freezing and thawing on the simulation results, we focus only on the summer period in the present study. For the Arou Station, we used the observations during June 1, 2014-September 30, 2014, during which the total precipitation was 503.6 mm and the average temperature was 9.1 °C. For the Shuanghu Station, we used the observations during June 1, 2015-September 30, 2015, during which the total precipitation was 181.6 mm and the average temperature was 5.6 °C.

We derived z_{om} using the mean vegetation height (*h*) as *h*/10 in each station. Based on the field observation in growing season, *h* are taken as 0.2 m and 0.03 m in Arou Station and Shuanghu Station, respectively. It should be noted that we did not consider the changes in vegetation height within growing season since this may be marginal in the grassland ecosystem. In terms of soil stratification, the Arou Station (alpine meadow) was divided into four soil layers with depth of 0.08 m, 0.24 m, 0.96 m, and 0.64 m in each layer, respectively; and the Shuanghu Station (alpine steppe) was also divided into four layers with depth of 0.1 m, 0.2 m, 0.2 m, and 0.6 m, respectively. For the root layers, we used the first three soil layers as the root layers. The soil and vegetation parameters (except LAI) used in Noah-MP are based on the results from field observations, while the LAI comes from the satellite observations and varies across months.

Noah-MP has multiple choices for numerous physical processes (Niu et al., 2011; He et al., 2023). The present study mostly used the default setting similar to Ma et al. (2017) except following ones: Jarvis (1976) scheme for canopy stomatal resistance; monthly dynamic LAI to calculate vegetation fraction; the original Noah scheme for the soil moisture factor for stomatal resistance (Ek et al., 2003); the Chen et al. (1997) scheme for surface layer drag/exchange coefficient; and; partitioning precipitation into rainfall & snowfall based on whether air temperature at the reference height less than freezing point (Niu et al., 2011). With above options, we ran Noah-MP at the half-hourly time step using the observed meteorological forcing including air temperature, air pressure, wind

speed, relative humidity, downward short- and long-wave radiation, and precipitation in each station. To spin-up the model, we first repeatedly ran the model 9 times and then kept only the 10th simulation for analysis.

For the purpose of model evaluations, we used the observed half-hourly R_n, H and λE in each station as references, the latter two were measured by the eddy-covariance flux tower. Note that the eddy-covariance observed H and λE may have larger uncertainties in certain circumstances (e.g., at night with weak turbulence). Therefore, we only used the good quality H and λE (marked by the EddyPro Software in data processing) in the model evaluations. The days with less than 36 half-hourly good quality H and λE data were removed from any evaluations.

For statistics, the root-mean-square error (RMSE), the mean absolute error (MAE), and the Nash-Sutcliffe efficiency (NSE) criterion were applied to evaluate the modeling results against the observations.

2.5. Modeling experiments design

2.5.1. Testing the new parameterization schemes

For each station, two simulation experiments were carried out with identical forcing and parameter values as inputs. The first simulation experiment (referred to as EXP1) utilized the model's default parameterization scheme [i.e., $C_{zil} = 0.1$ and Eq. (7) for the homogeneous root distribution], whereas the second simulation experiment (referred to as EXP2) incorporated the new parameterization schemes for z_{oh} with a more universal C_{zil} (Eq. 3) and the asymptotic nonlinear root distribution (Eq. 9). The comparisons between EXP2 and EXP1 therefore illustrate the usefulness of the new parameterization schemes in these two ecosystems.

2.5.2. Multi-scenario modeling experiments with varying meteorological forcing

Using the modified Noah-MP with two new parameterization schemes, we further design three groups of modeling with different meteorological forcing scenarios to explore the possible impacts of future climate change on land evapotranspiration in two alpine ecosystems. Note that the multi-scenario modeling experiments all used the two new parameterization schemes for z_{oh} and root distribution. That is, the EXP2 is regarded as the "control" modeling experiment. Based on EXP2, three groups experiments are further implemented, which include: (i) Precipitation experimental group: keeping other inputs unchanged and perturb the observed precipitation by − 75%, − 50%, − 25%, − 10%, 10%, 25%, 50%, and 75%, respectively; (ii) Solar radiation experimental group: keeping other inputs unchanged and perturb the observed solar radiation at − 15%, − 10%, − 5%, − 5%, 2%, 2%, 5%, 10% and 15%, respectively; and, (iii) Air temperature experimental group: keep other inputs unchanged and perturb the observed air temperature by − 2 °C, − 1.5 °C, − 1 °C, − 0.5 °C, 0.5 °C, 1 °C, 1.5 °C, and 2 °C, respectively (In all experiments, the minus sign means "decrease", while the positive sign means "increase"). For each scenario, the modelled ET, E_s and T_r are all compared with those from EXP2 to quantify their relative changes.

3. Results

3.1. Evaluation of two new parameterization schemes

3.1.1. Alpine meadow

Fig. 2 shows the daily mean observed and simulated R_n, H and λE in the Arou Station (alpine meadow) during the period of 1 June-30 September 2014. Overall, compared to observations, Noah-MP can simulate the intra-annual variations of R_n and λE in the alpine meadow when the default parameterization schemes are used (i.e., EXP1), but it obviously overestimates both fluxes (Fig. 2 & 3). For H, the default Noah-MP tends to overestimate it in June and July, but underestimates it in August and September. The diurnal variations illustrated in Fig. 3c suggests the modeled λE grows very fast in the morning, resulting in overestimated λE being significantly larger than the observations at noon in EXP1 (e.g., the error can be more than 30 W m^{-2} in July and August). When the modified C_{zil} and root distribution were employed in the Noah-MP (i.e., EXP2), the overestimation of R_n and λE could be significantly mitigated (Fig. 2 & 3). For example, the λE simulated by EXP1 appear much larger than the observed values during late-June to mid-June and September, while such an overestimation is greatly mitigated in EXP2 (Fig. 2c). The improvements are also true for R_n, as can be seen from the lower errors at noon in EXP2 (Fig. 3a), which are particularly obvious in June and September. For the H, because the new z_{oh} scheme decreases the surface exchange coefficient for heat transfer, the positive biases during June and July in alpine meadow have also been reduced to some extent in EXP2 (Fig. 3b). However, H during August and September was underestimated in EXP1, the new z_{oh} scheme causes more negative biases in these two months (Fig. 3b), leading to marginal improvements in H for the whole period (Table 1).

Overall, by comparing the two modeling experiments in the alpine meadow for the daily values (Table 1), the NSE value for λE has been improved from 0.847 (EXP1) to 0.902 (EXP2) and the NSE value for R_n has been improved from 0.982 (EXP1) to 0.989 (EXP2), while for H the NSE value even becomes degraded to some extent because of the reasons explained above. This is mainly because the improved parameterization schemes for asymptotic nonlinear root distribution are mostly effective for water exchanges (λE), while the new parameterization scheme for z_{oh} can only mitigate the positive bias in H in the alpine meadow.

3.1.2. Alpine steppe

Fig. 4 shows the daily mean values of observed and simulated R_n, H and λE for the period 1 June-30 September 2015 for the Shuanghu Station (alpine steppe). In contrast to above alpine meadow, Noah-MP in EXP1 significantly underestimated R_n and λE in alpine steppe with mean absolute errors of 13.26 and 25.77 W m^{-2}, respectively, while it also remarkably overestimated H with mean
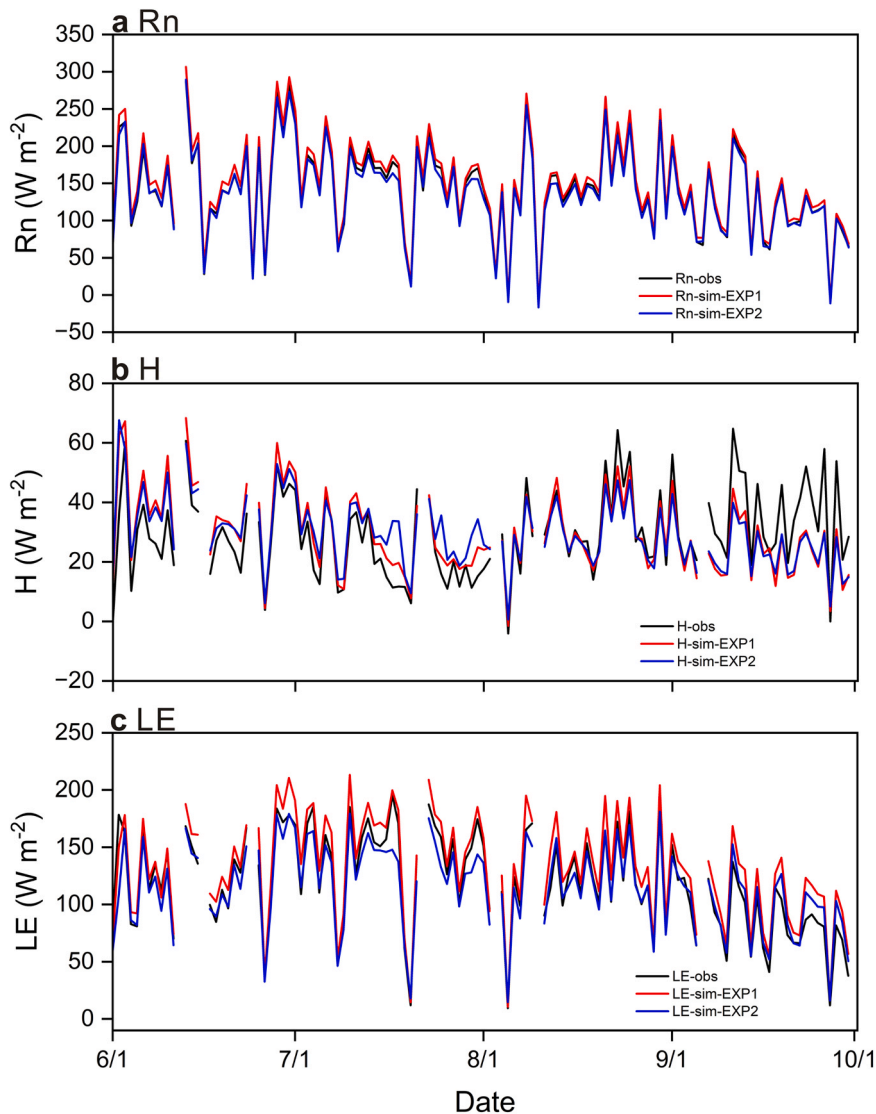
Fig. 2. Comparison of daily mean net radiation (R_n), sensible (H) and latent (λE) heat flux from the EXP1 and EXP2 simulations against in-situ observations in the Arou Station with alpine meadow (June 1-September 30, 2014).

absolute error of 36.01 W m^{-2}. At the diurnal scale (Fig. 5), H was significantly overestimated during the daytime, while λE during daytime was largely underestimated. The NSE values of H and λE from EXP1 are even negative (Table 2), indicating that Noah-MP has a greater challenge in modeling the energy fluxes in the alpine steppe with a more arid climate. Moving to EXP2 with two new parameterization schemes, the modeling errors in H are substantially reduced, leading to much lower MAE (15.0 W m^{-2}) and RMSE (17.86 W m^{-2}) values comparing to EXP1 (Table 2). However, the accuracies in the R_n and λE simulated by EXP2 are still similar to those by EXP1 (Fig. 4 & 5).

Overall, by comparing the two modeling experiments in the alpine steppe for the daily values (Table 2), the NSE value for H has been largely improved from $-$ 4.358 (EXP1) to $-$ 0.082 (EXP2), but the NSE value for R_n has been greatly decreased from 0.738 (EXP1) to $-$ 0.578 (EXP2), while the difference in NSE values for λE between two experiments is marginal. This implies that the new parameterization schemes for the root distribution cannot improve the accuracy in the modeled λE and R_n in the alpine steppe, while the new parameterization scheme for z_{oh} plays a key role in mitigating the modeling error in H in this ecosystem.

3.2. Responses of evapotranspiration to varying meteorological conditions

3.2.1. Alpine meadow

In terms of the Arou Station with alpine meadow, the ET, E_s and T_r simulated by EXP2 for the period of 1 June-30 September 2014 were 370.2 mm, 117.3 mm and 220.8 mm, respectively, while the precipitation during this period was 503.6 mm. This indicates this
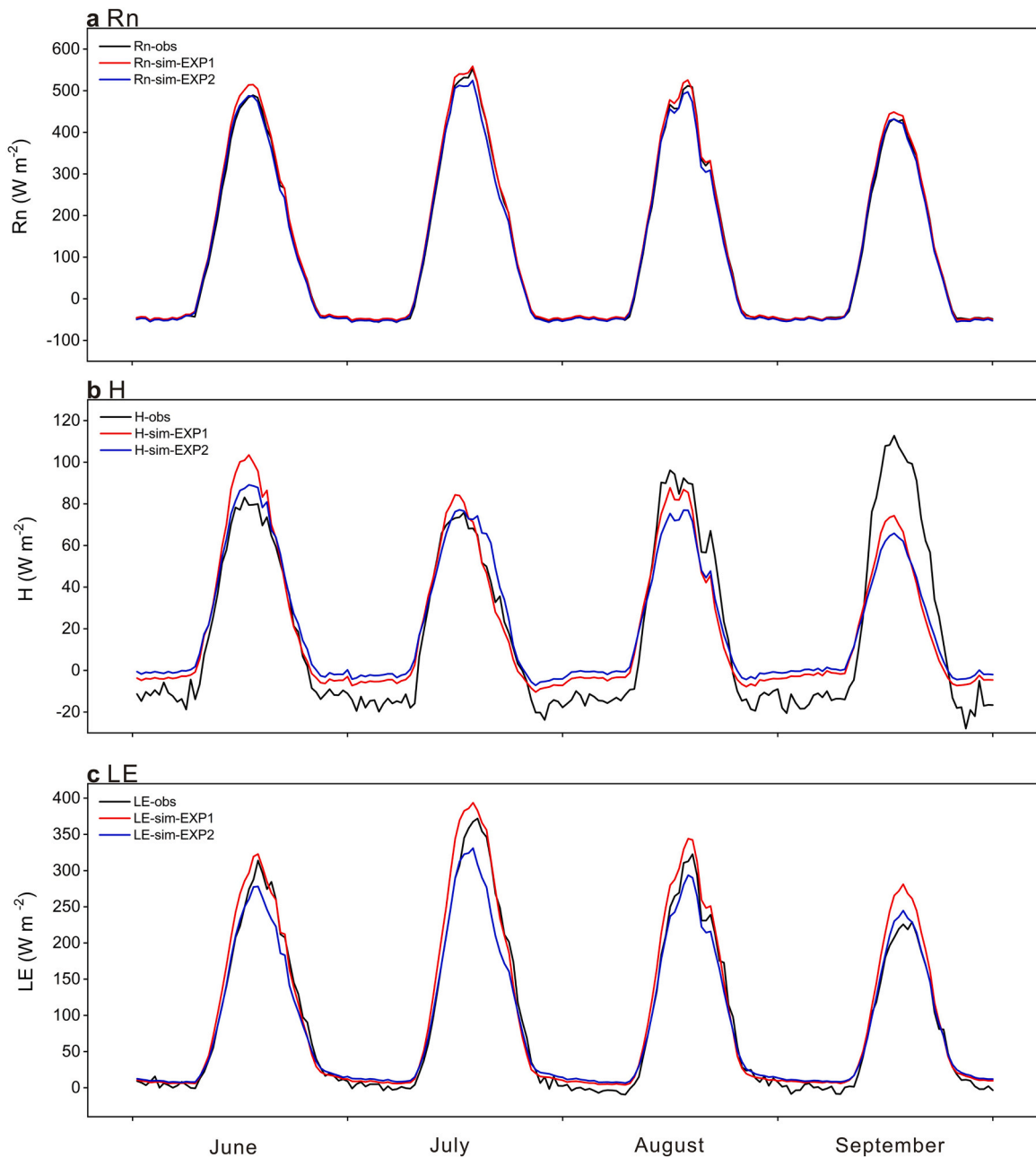
Fig. 3. Comparison of the monthly mean half-hourly net radiation (R_n), sensible (H) and latent (λE) heat flux from EXP1 and EXP2 simulations against in-situ observations in the Arou Station with alpine meadow (June 1-September 30, 2014).

ecosystem is relatively wet with substantial soil water. Fig. 6 shows the responses of ET, E_s and T_r to varying precipitation, solar radiation and air temperature in the alpine meadow. As seen, the ET and its components vary little when precipitation increases (Fig. 6a). This is probably due to the abundance of soil moisture and the limitation of the atmospheric demand, thus increasing precipitation does not further affect ET. However, when the precipitation decreases, ET and its components respond quickly. For example, ET, E_s and T_r decrease by − 53.7%, − 63.8%, and − 55.1%, respectively, when precipitation decreases by − 75%, suggesting that possible future extreme droughts event may lead to a significant negative impact on the alpine meadow ecosystem.

In terms of solar radiation (Fig. 6b), ET, E_s and T_r from alpine meadow positively respond to increased available energy resulting from increased solar radiation. For example, when the solar radiation increases by 10%, ET, E_s and T_r increase by 8.6%, 13.3%, and 6.6%, respectively, suggesting that the E_s is more sensitive to solar radiation than the T_r. With regard to air temperature (Fig. 6c), changes in ET in alpine meadow are particularly weak no matter how much warming or cooling occurs. For example, the changes in

Table 1

Statistical metrics of the daily R_n, H and λE from the EXP1 and EXP2 simulations in the Arou Station with alpine meadow.

	R_n		H		λE	
	EXP1	EXP2	EXP1	EXP2	EXP1	EXP2
MAE (W m^{-2})	7.41	5.07	7.07	7.72	14.49	9.46
RMSE (W m^{-2})	8.38	6.34	9.10	10.23	16.88	13.45
NSE	0.982	0.989	0.609	0.506	0.847	0.902

ET, E_s and T_r are all less than 3% for a 2 °C increase in air temperature. This may be due to the fact that changing temperature inputs alone did not change precipitation and solar radiation, leading to little impact on the evapotranspiration processes.

3.2.2. Alpine steppe

Fig. 7 shows the responses of ET, E_s and T_r to varying precipitation, solar radiation and air temperature in the Shuanghu Station with alpine steppe. The actual precipitation from 1 June to 30 September 2015 was 181.6 mm, while the ET, E_s and T_r from EXP2 over a same period are 109. 8 mm, 87.9 mm, 18.7 mm, respectively. Note that such modelled results were much smaller than the observed
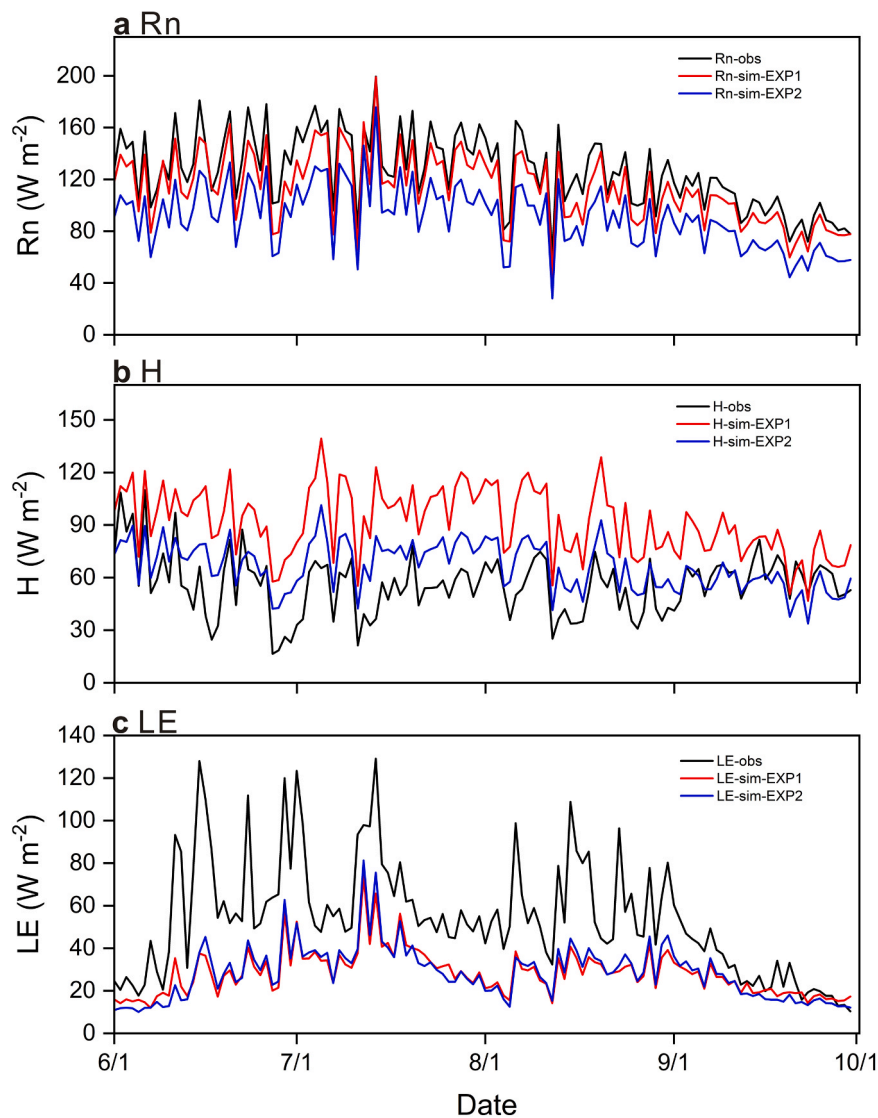

Fig. 4. Comparison of daily mean net radiation (Rn), sensible (H) and latent (λE) heat flux from the EXP1 and EXP2 simulations against in-situ observations in the Shuanghu Station with alpine steppe (June 1-September 30, 2015).
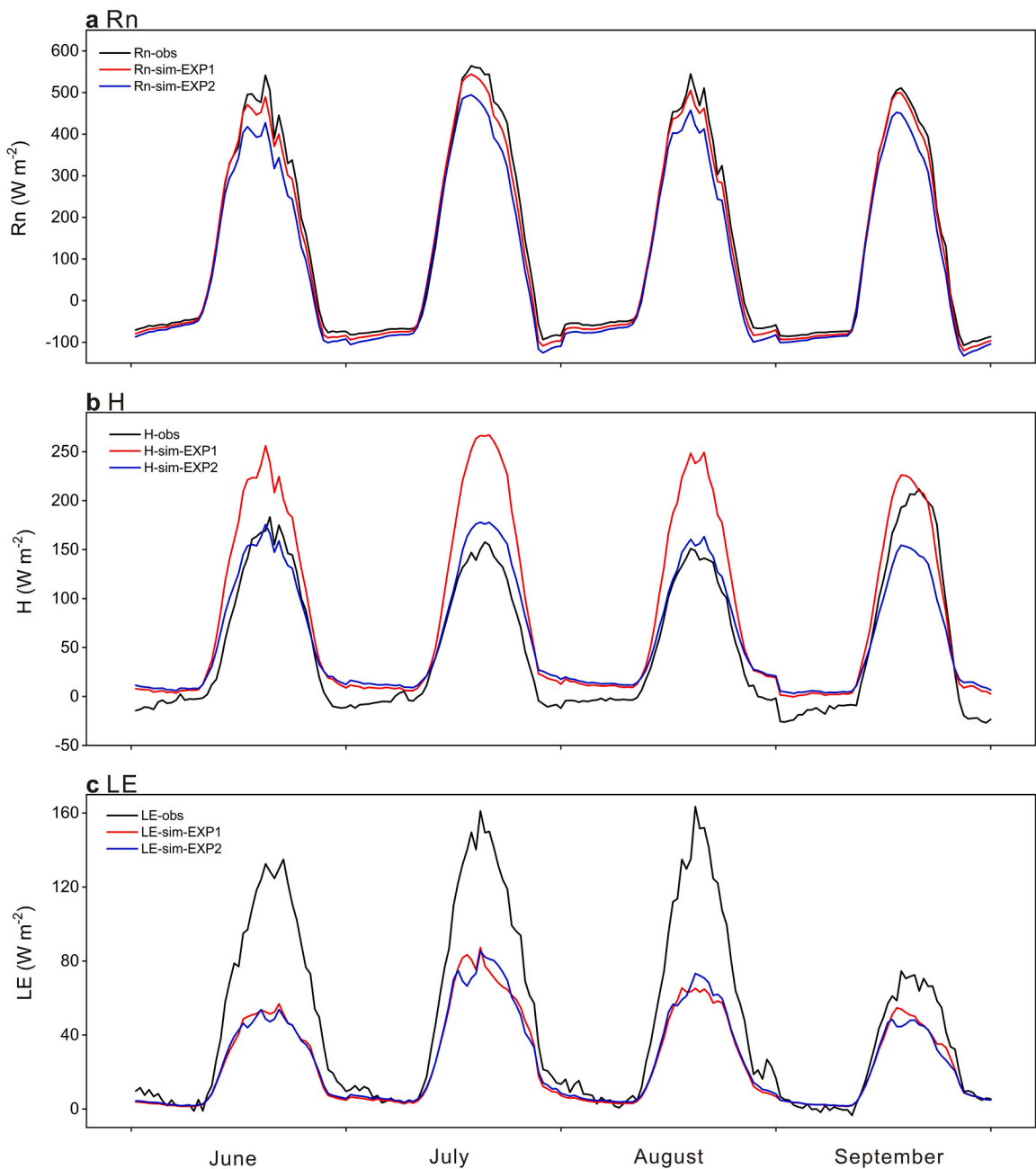
Fig. 5. Comparison of the monthly mean half-hourly net radiation (Rn), sensible (H) and latent (λE) heat flux from EXP1 and EXP2 simulations against in-situ observations in the Shuanghu Station with alpine steppe (June 1-September 30, 2015).

values. From the multi-scenario modeling experiments, it is found that when precipitation increases, both ET and E_s increase, e.g., a 75% increase in precipitation could cause ET and E_s increase by 23.2% and 28.9%, respectively (Fig. 7a). However, ET and E_s in alpine steppe are more sensitive to decreasing precipitation (Fig. 7a), as can be seen that a − 75% decrease in precipitation could lead to − 52.6% and − 62.3% decreases in ET and E_s, respectively. However, the impact of changing precipitation in T_r in alpine steppe appears to be much marginal (Fig. 7a), as can be seen that T_r varies little no matter how much precipitation changes. This is because the vegetation coverage in alpine steppe is much less than that in alpine meadow, thus the ratio of T_r to ET is much smaller (Ma and Zhang, 2022b). This also explains why the responses of E_s to changing precipitation are much similar to those of ET since soil evaporation is the primary contributor of ET in alpine steppe.

Similar to alpine meadow, ET and E_s positively response to increasing solar radiation, as can be seen that a 10% increase in solar radiation causes that ET and E_s increase by 5.8% and 8.9%, respectively (Fig. 7b). The responses of ET and its components to changing

Table 2

Statistical metrics of the daily R_n, H and λE from the EXP1 and EXP2 simulations in the Shuanghu Station with alpine steppe.

	R_n		H		λE	
	EXP1	EXP2	EXP1	EXP2	EXP1	EXP2
MAE (W m^{-2})	13.26	35.59	36.01	15.0	25.77	25.42
RMSE (W m^{-2})	14.85	36.43	39.74	17.86	16.88	11.44
NSE	0.738	−0.578	−4.358	−0.082	−0.451	−0.372

air temperature in alpine steppe are also similar to those in alpine meadow. The changes in ET and E_s are all less than 4% for a 2 °C increase in air temperature (Fig. 7c).

Interestingly, T_r in the alpine steppe decreases significantly when the air temperature increases. A possible explanation is that increased air temperature alone lead to higher vapor pressure deficit, which partly reduces the stomatal conductance in such an arid region. It should be emphasized that the response of T_r to air temperature in alpine steppe appears to be more remarkable than that in alpine meadow (comparing Figs. 6c and 7c), suggesting the former may be more vulnerable to future warming than the latter. In fact, the previous study on the phenology of alpine grassland by Shen et al. (2015) has demonstrated that the starting date of growing season of alpine steppe in western TP did not advance even though there were significant warming in the past few decades, which is much different with the alpine meadow in the eastern TP with earlier green-up dates.
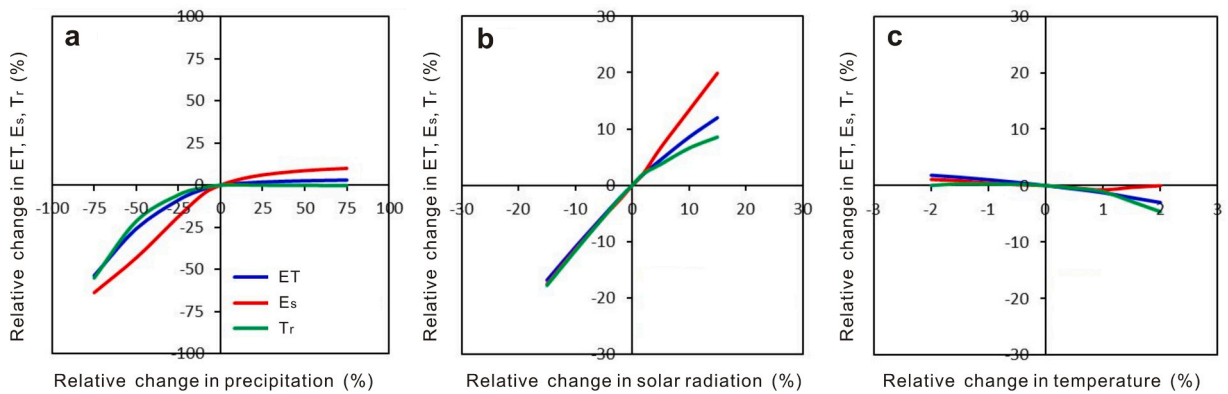

Fig. 6. Reponses of evapotranspiration (ET), soil evaporation (E_s) and transpiration (T_r) to (a) precipitation, (b) solar radiation and (c) temperature changes in the Arou Station with alpine meadow. The precipitation varies by − 75%, − 50%, − 25%, − 10%, 10%, 25%, 50% and 75%, respectively; the solar radiation varies by − 15%, − 10%, − 5%, − 2%, 2%, 5%, 10% and 15%, respectively; the temperature varied by − 2 °C, − 1.5 °C, − 1 °C, − 0.5 °C, 0.5 °C, 1 °C, 1.5 °C and 2 °C, respectively.
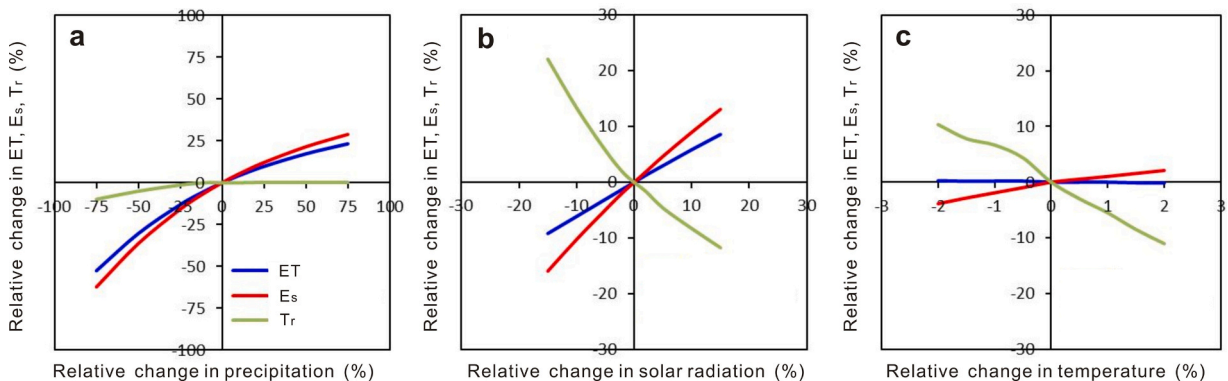

Fig. 7. Reponses of evapotranspiration (ET), soil evaporation (E_s) and transpiration (T_r) to (a) precipitation, (b) solar radiation and (c) temperature changes in the Shuanghu Station with alpine steppe. The precipitation varies by − 75%, − 50%, − 25%, − 10%, 10%, 25%, 50% and 75%, respectively; the solar radiation varies by − 15%, − 10%, − 5%, − 2%, 2%, 5%, 10% and 15%, respectively; the temperature varied by − 2 °C, − 1.5 °C, − 1 °C, − 0.5 °C, 0.5 °C, 1 °C, 1.5 °C and 2 °C, respectively.

4. Discussions

4.1. Reasons for different performances with new parameterization schemes in two ecosystems

The sensitivity analysis by Li et al. (2018) suggested that the vegetation height is the most sensitive vegetation parameter in Noah-MP that greatly affects the modeled energy fluxes in TP. In this way, one of modifications in the present study is to take the canopy height into account in estimating the roughness length for both heat and momentum transfers. Using the real vegetation height measured in the field, the C_{zil} becomes 0.83 and 0.97 for the alpine meadow and alpine steppe, respectively, which are much higher than the default value of 0.1. These new C_{zil} values reduce the z_{oh}, thus decreasing the surface exchange coefficient for heat transfer (Chen and Zhang, 2009). This explains why the overestimation of H can be mitigated in both ecosystems (Figs. 2–5), particularly for the alpine steppe (Figs. 4–5). However, the H in alpine meadow was to some extent underestimated during August and September even with the original $C_{zil} = 0.1$, the skill of Noah-MP in modeling H thus becomes worse when new z_{oh} scheme is used. This indicates that, in addition to bias in the surface exchange coefficient for heat transfer, the possible error in the modeled land surface temperature may be another key reason for the overestimation in H in alpine meadow (Zheng et al., 2014), which deserves further investigations.

The different effects of asymptotic nonlinear root distribution on the modelled λE between alpine meadow and alpine steppe can be attributed to the different roles of plant transpiration in ET. In theory, a more realistic root distribution can better describe the root water uptake process (Wang et al., 2018; Zheng et al., 2015c), thereby improving the accuracy in plant transpiration modeling. For example, Wang et al. (2022a) found that the error in the modeled ET from the Hydrus-1D could be reduced by approximately 39% using a more authentic root distribution from the original the generic root profile. In the alpine meadow, the plant transpiration is the main contributor of ET (Cui et al., 2020; Zhu et al., 2013), thus the new parameterization scheme of asymptotic nonlinear root distribution obviously mitigates the error in λE. However, in the alpine steppe with a more arid climate, the plant transpiration is particularly marginal because of sparse vegetation coverage (Ma and Zhang, 2022b; Ma et al., 2015a). Consequently, the modification of root distribution cannot lead to much improvements in the modeled λE over alpine steppe because the bias in the soil evaporation may be still large. It should be noted that the new root distribution scheme implemented in this study remains a "static" root. In nature, however, the plants are able to adapt to changing environments and, thus, may have dynamic roots to better absorb water to survive. For example, by incorporating a vegetation optimality model into Noah-MP, Wang et al. (2018) explicitly showed the significance of deep roots for simulating the water uptake and ET of phreatophytes in arid regions. Recently, Niu et al. (2020) improved Noah-MP by developing an explicit representation of plant water storage supplied by dynamic root water uptake through hydrotropic root growth to meet the transpiration demand, which largely improves the accuracy in the evapotranspiration and ecosystem productivity. While testing this new dynamic root parameterization is beyond the scope the present study, we argue that a reasonable representation of root is key to ET modeling in alpine grassland in TP.

4.2. Comparisons with previous studies for land surface modeling in TP

While Wang et al. (2022b) employed Noah-MP to simulate H and λE across the whole TP over the past three decades, previous studies also reported certain deficiency in Noah-MP in land surface modeling in this special region. In particular, there are numerous studies dedicating into understanding the physical processes related to soil water and heat processes in Noah-MP. For example, Gao et al. (2015) found that considering the changes in saturated hydraulic conductivity due to root could substantially improve the accuracies in both topsoil moisture and turbulent fluxes, while Li et al. (2020) suggested that a more reliable frozen soil thermal conductivity could improve the deep soil temperature estimation in the permafrost region of TP. In the present study, we found that a better representation of the roughness length for heat transfer could largely improve the accuracy in the H, which is particularly apparent in the alpine steppe (Fig. 5). This is supported by a recent study in the alpine meadow of the Heihe River basin (Sun et al., 2022), which found that the surface exchange coefficient for heat transfer is one of the most important physical processes that determines the performance of Noah-MP.

The present study found that a more realistic representation of root distribution could improve λE simulations in the alpine meadow in the upper reach of Heihe River Basin, which is consistent with the findings of Zheng et al. (2015c) in the source region of the Yellow River Basin. In fact, Gao et al. (2015) and Zheng et al. (2015c) were probably the first few studies that evaluated the Noah-MP in the typical alpine meadows in TP. However, little information about Noah-MP is known for another major ecosystem in TP, i.e., alpine steppe. The present study found that, even with new parameterization schemes, Noah-MP still has a greater challenge in modeling the land-atmosphere energy and water exchanges in alpine steppe than that in alpine meadow, as can be seen from the larger biases in both H and λE in the former ecosystem (Figs. 4-5). In particular, the deficiency in λE is due mostly to the error in the modeled soil evaporation since plant transpiration plays a minor role in alpine steppe. Previous studies (Yang et al., 2009a) have suggested that improving representation of soil water flow and the soil surface resistance in the SiB2 land surface model could largely improve the accuracy in the soil moisture in the desert area, which provides an important clue for future modification of Noah-MP in the alpine steppe with a relatively arid climate.

Understanding how ET responses to climate factors is of importance for predicting the impact of changing environment on hydrological cycle (Fisher et al., 2017; Ma et al., 2021). While there have been a wide range of studies on how climate/vegetation changes impact ET from TP (e.g., Ma and Zhang, 2022b), most of them focus only on the real changes in climate/vegetation during the historical period, failing to represent the impact of extreme climate on ET. In this context, the present study used the modified Noah-MP to implement modeling experiments with multi-scenario meteorological forcing. The scenarios even include a three fourth decrease in precipitation and a 2 °C increase in air temperature, which enable us to know the impacts of possible extreme climate (e.g., severe

drought or heatwave) on the water transfer process across the soil-vegetation-atmosphere continuum in these alpine ecosystems. In particular, we found that the alpine steppe may be more vulnerable to future warming than the alpine meadow, thus indicating that more effective strategies are needed from the decision-makers to maintain the ecological balance in the central and western TP under a more fragile environment. Note that it has been reported that, in addition to significant changes in temperature and precipitation (Yao et al., 2019; Yang et al., 2014), TP also witnessed obvious wind stilling (Zhang and Wang, 2020) and increasing vapor pressure deficit (Ding et al., 2018) in past few decades. However, the present modeling experiments only focus on three climatic factors (i.e., precipitation, temperature and solar radiation), while the influences from other environmental factors such as wind and humidity are not considered. Future studies are encouraged to dedicate into more understanding of how these factors impact ET in such a region.

4.3. Limitations in the present study

There are still a few limitations in the present study. Firstly, the primary merit of Noah-MP is it has multiple choices for a wide range of physical processes (Niu et al., 2011). This enables the community to evaluate the role of different physical processes in controlling the land surface fluxes and the associate states (Li et al., 2022; Zhang et al., 2016). By identifying the sensitive processes, it is also possible to find out the optimal combinations for different physical processes that yield the "best" skill of Noah-MP in land surface modeling, as has been done by, e.g., Chang et al. (2020) and Li et al. (2022). However, the present study mostly used the default options suggested by Niu et al. (2011) and Ma et al. (2017) with only slight modifications (see Section 2.4). Moreover, only two processes, i.e., the surface exchange coefficient for heat transfer and the root water update, are investigated in this study. Therefore, further investigations on other physical processes (e.g., those related to soil water and land surface temperature) remain urgently needed for an improved land surface modeling in the alpine grassland in TP. Secondly, in addition to model structure, the parameter values also play a key role in determining the model's performance. For example, Li et al. (2018) found that soil parameters are overall more important than the vegetation parameters in central TP because of the limited photosynthetic processes in sparse vegetations. Cuntz et al. (2016) found that the Noah-MP's hydrologic output fluxes from Noah-MP are sensitive to two thirds of its applicable standard parameters, indicating a through calibration of parameter values against observations may be a key step to further improve the model's skill in future. However, the present study basically used the default parameter values of Noah-MP without calibration. Thus, it is believed that the biases in the modeled energy fluxes identified here can also be largely mitigated by parameter optimization. Last but not least, the present ET partitioning from Noah-MP has not been validated due to lack of measured data on E_s and T_r (Cui et al., 2020). Therefore, the responses of ET and its components to changing climate quantified in this study may have some uncertainties. In future, in-situ observations of soil evaporation and vegetation transpiration are needed to facilitate a more thorough evaluation of land surface modeling in Tibetan Plateau.

5. Conclusions

This study employed the third-generation land surface model, Noah-MP, to simulate the land-atmosphere energy and water exchanges in two typical land cover types (alpine meadow and alpine steppe) in Tibetan Plateau. It is found that the default Noah-MP largely overestimates (underestimates) R_n and λE, but mostly underestimates (overestimates) H in alpine meadow (alpine steppe). By coupling the new parameterization schemes for the roughness length for heat transfer (z_{oh}) and the asymptotic nonlinear root distribution into Noah-MP, the errors in the modeled R_n and λE in alpine meadow can be largely mitigated, but little improvement is seen for H. In the alpine steppe, however, substantial improvement in the H is achieved when the new parameterization schemes are implemented, though they appear less effective in reducing errors in the modeled R_n and λE. In general, we found that there is a greater room for further improving Noah-MP in the alpine steppe with an arid climate in future.

Using multi-scenario simulations of Noah-MP, the responses of ET and its two components (i.e., E_s and T_r) to changes in precipitation, solar radiation and air temperature are also quantified. In the alpine meadow, ET, E_s and T_r are much more sensitive to decreasing precipitation than that to increasing precipitation. This is because the abundant soil moisture makes alpine meadow not sensitive to further increasing water replenishment. In the alpine steppe, the responses of ET and E_s to changing precipitation are similar to those in alpine meadow, but the T_r varies little no matter how much precipitation varies since the plant transpiration is rather small in such an ecosystem. The responses of ET and its components to changing air temperature are weak in both alpine steppe and alpine meadow, as can be seen that changes in ET from both ecosystems are within 4% even though air temperature increased by 2 °C. However, the T_r shows negative responses to increased temperature and such responses in alpine steppe appear to be more remarkable than those in alpine meadow, suggesting the former may be more vulnerable to future warming than the latter.

CRediT authorship contribution statement

Ma Ning: Writing – review & editing, Writing – original draft, Investigation, Funding acquisition, Formal analysis, Data curation, Conceptualization, Visualization.

Declaration of Competing Interest

The authors declare that they have no known competing financial interests or personal relationships that could have appeared to influence the work reported in this paper.

Data availability

Data will be made available on request.

Acknowledgements

References

Bonan, G.B., Doney, S.C., 2018. Climate, ecosystems, and planetary futures: the challenge to predict life in Earth system models. Science 359. https://doi.org/10.1126/science.aam8328.

Bonan, G.B., Lawrence, P.J., Oleson, K.W., Levis, S., Jung, M., Reichstein, M., Lawrence, D.M., Swenson, S.C., 2011. Improving canopy processes in the Community Land Model version 4 (CLM4) using global flux fields empirically inferred from FLUXNET data. J. Geophys. Res. 116 https://doi.org/10.1029/2010jg001593.

Cai, X., Yang, Z.-L., Xia, Y., Huang, M., Wei, H., Leung, L.R., Ek, M.B., 2014. Assessment of simulated water balance from Noah, Noah-MP, CLM, and VIC over CONUS using the NLDAS test bed. J. Geophys. Res.: Atmospheres 119, 13751–13770. https://doi.org/10.1002/2014JD022113.

Chang, M., Liao, W., Wang, X., Zhang, Q., Chen, W., Wu, Z., Hu, Z., 2020. An optimal ensemble of the Noah-MP land surface model for simulating surface heat fluxes over a typical subtropical forest in South China. Agric. For. Meteorol. 281, 107815 https://doi.org/10.1016/j.agrformet.2019.107815.

Chen, F., Dudhia, J., 2001. Coupling an advanced land surface-hydrology model with the Penn State-NCAR MM5 modeling system. Part I: model implementation and sensitivity. Mon. Weather Rev. 129, 569–585.

Chen, F., Zhang, Y., 2009. On the coupling strength between the land surface and the atmosphere: from viewpoint of surface exchange coefficients. Geophys. Res. Lett. 36 https://doi.org/10.1029/2009gl037980.

Chen, F., Janjic, Z., Mitchell, K.E., 1997. Impact of atmospheric surface-layer parameterizations in the new land-surface scheme of the NCEP Mesoscale Eta Model. Bound. -Layer. Meteorol. 85, 391–421.

Chen, Y., Yang, K., Zhou, D., Qin, J., Guo, X., 2010. Improving the Noah land surface model in arid regions with an appropriate parameterization of the thermal roughness length. J. Hydrometeorol. 11, 995–1006. https://doi.org/10.1175/2010jhm1185.1.

Clark, M.P., Fan, Y., Lawrence, D.M., Adam, J.C., Bolster, D., Gochis, D.J., Hooper, R.P., Kumar, M., Leung, L.R., Mackay, D.S., Maxwell, R.M., Shen, C., Swenson, S.C., Zeng, X., 2015. Improving the representation of hydrologic processes in Earth System Models. Water Resour. Res. 51, 5929–5956. https://doi.org/10.1002/2015wr017096.

Clark, M.P., Bierkens, M.F.P., Samaniego, L., Woods, R.A., Uijlenhoet, R., Bennett, K.E., Pauwels, V.R.N., Cai, X., Wood, A.W., Peters-Lidard, C.D., 2017. The evolution of process-based hydrologic models: historical challenges and the collective quest for physical realism. Hydrol. Earth Syst. Sci. 21, 3427–3440. https://doi.org/10.5194/hess-21-3427-2017.

Cosgrove, B., Gochis, D.J., Clark, E., Cui, Z., Dugger, A., Feng, X., Khan, S., 2017. Continental-scale operational hydrologic modeling: Version 1.0 of the National Water Model. Paper presented at 97th American Meteorological Society Annual Meeting, American Meteorological Society, Seattle, WA. Retrieved from ⟨https://ams.confex.com/ams/97Annual/webprogram/Paper314045.html⟩.

Cui, J., Tian, L., Wei, Z., Huntingford, C., Wang, P., Cai, Z., Ma, N., Wang, L., 2020. Quantifying the controls on evapotranspiration partitioning in the highest alpine meadow ecosystem. e2019WR024815 Water Resour. Res. 56. https://doi.org/10.1029/2019wr024815.

Cuntz, M., Mai, J., Samaniego, L., Clark, M., Wulfmeyer, V., Branch, O., Attinger, S., Thober, S., 2016. The impact of standard and hard-coded parameters on the hydrologic fluxes in the Noah-MP land surface model. J. Geophys. Res.: Atmospheres 121, 10676–10700. https://doi.org/10.1002/2016jd025097.

Ding, J., Yang, T., Zhao, Y., Liu, D., Wang, X., Yao, Y., Peng, S., Wang, T., Piao, S., 2018. Increasingly important role of atmospheric aridity on Tibetan alpine grasslands. Geophys. Res. Lett. 45, 2852–2859. https://doi.org/10.1002/2017gl076803.

Ek, M.B., Mitchell, K.E., Lin, Y., Rogers, E., Grunmann, P., Koren, V., Gayno, G., Tarpley, J.D., 2003. Implementation of Noah land surface model advances in the National Centers for Environmental Prediction operational mesoscale Eta model. J. Geophys. Res. 108 https://doi.org/10.1029/2002jd003296.

Fisher, J.B., Melton, F., Middleton, E., Hain, C., Anderson, M., Allen, R., McCabe, M.F., Hook, S., Baldocchi, D., Townsend, P.A., Kilic, A., Tu, K., Miralles, D.D., Perret, J., Lagouarde, J.-P., Waliser, D., Purdy, A.J., French, A., Schimel, D., Famiglietti, J.S., Stephens, G., Wood, E.F., 2017. The future of evapotranspiration: global requirements for ecosystem functioning, carbon and climate feedbacks, agricultural management, and water resources. Water Resour. Res. 53, 2618–2626. https://doi.org/10.1002/2016wr020175.

Fisher, R.A., Koven, C.D., 2020. Perspectives on the future of land Surface Models and the challenges of representing complex terrestrial systems. J. Adv. Model. Earth Syst. 12 https://doi.org/10.1029/2018ms001453.

Gale, M.R., Grigal, D.F., 1987. Vertical root distributions of northern tree species in relation to successional status. Can. J. For. Res. 17, 829–834.

Gao, Y., Li, K., Chen, F., Jiang, Y., Lu, C., 2015. Assessing and improving Noah-MP land model simulations for the central Tibetan Plateau. J. Geophys. Res.: Atmospheres 120, 9258–9278. https://doi.org/10.1002/2015jd023404.

He, C., Valayamkunnath, P., Barlage, M., Chen, F., Gochis, D., Cabell, R., Schneider, T., Rasmussen, R., Niu, G.-Y., Yang, Z.-L., Niyogi, D., Ek, M., 2023. Modernizing the open-source community Noah with multi-parameterization options (Noah-MP) land surface model (version 5.0) with enhanced modularity, interoperability, and applicability. Geosci. Model Dev. 16, 5131–5151. https://doi.org/10.5194/gmd-16-5131-2023.

Huang, J., Zhou, X., Wu, G., Xu, X., Zhao, Q., Liu, Y., Duan, A., Xie, Y., Ma, Y., Zhao, P., Yang, S., Yang, K., Yang, H., Bian, J., Fu, Y., Ge, J., Liu, Y., Wu, Q., Yu, H., Wang, B., Bao, Q., Qie, K., 2023. Global climate impacts of land-surface and atmospheric processes over the Tibetan Plateau. Rev. Geophys. 61 https://doi.org/10.1029/2022rg000771.

Jarvis, P.G., 1976. The interpretation of the variations in leaf water potential and stomatal conductance found in canopies in the field. Philos. Trans. R. Soc. Lond. B, Biol. Sci. 273, 593–610.

Li, J., Chen, F., Zhang, G., Barlage, M., Gan, Y., Xin, Y., Wang, C., 2018. Impacts of land cover and soil texture uncertainty on land model simulations over the Central Tibetan Plateau. J. Adv. Model. Earth Syst. 10, 2121–2146. https://doi.org/10.1029/2018MS001377.

Li, J., Miao, C., Zhang, G., Fang, Y.H., Shangguan, W., Niu, G.Y., 2022. Global evaluation of the Noah-MP land surface model and suggestions for selecting parameterization schemes. J. Geophys. Res.: Atmospheres 127, e2021JD035753. https://doi.org/10.1029/2021jd035753.

Li, X., Cheng, G., Liu, S., Xiao, Q., Ma, M., Jin, R., Che, T., Liu, Q., Wang, W., Qi, Y., Wen, J., Li, H., Zhu, G., Guo, J., Ran, Y., Wang, S., Zhu, Z., Zhou, J., Hu, X., Xu, Z., 2013. Heihe Watershed Allied Telemetry Experimental Research (HiWATER): scientific objectives and experimental design. Bull. Am. Meteorol. Soc. 94, 1145–1160. https://doi.org/10.1175/bams-d-12-00154.1.

Li, X., Wu, T., Zhu, X., Jiang, Y., Hu, G., Hao, J., Ni, J., Li, R., Qiao, Y., Yang, C., Ma, W., Wen, A., Ying, X., 2020. Improving the Noah-MP model for simulating hydrothermal regime of the active layer in the permafrost regions of the Qinghai-Tibet Plateau. J. Geophys. Res.: Atmospheres 125, e2020JD032588. https://doi.org/10.1029/2020jd032588.

Li, Y., Sun, R., Liu, S., 2014. Vegetation physiological parameter setting in the Simple Biosphere model 2 (SiB2) for alpine meadows in the upper reaches of Heihe river. Sci. China Earth Sci. 58, 755–769. https://doi.org/10.1007/s11430-014-4909-1.

Liang, J., Yang, Z.-L., Lin, P., 2019. Systematic hydrological evaluation of the Noah-MP land surface model over China. Adv. Atmos. Sci. 36, 1171–1187. https://doi.org/10.1007/s00376-019-9016-y.

Liu, S., Li, X., Xu, Z., Che, T., Xiao, Q., Ma, M., Liu, Q., Jin, R., Guo, J., Wang, L., Wang, W., Qi, Y., Li, H., Xu, T., Ran, Y., Hu, X., Shi, S., Zhu, Z., Tan, J., Zhang, Y., Ren, Z., 2018. The Heihe integrated observatory network: a basin-scale land surface processes observatory in China. Vadose Zone J. 17, 1–21. https://doi.org/10.2136/vzj2018.04.0072.

Lu, H., Zheng, D., Yang, K., Yang, F., 2020. Last-decade progress in understanding and modeling the land surface processes on the Tibetan Plateau. Hydrol. Earth Syst. Sci. 24, 5745–5758. https://doi.org/10.5194/hess-24-5745-2020.

Ma, N., Zhang, Y., 2022a. Contrasting trend in water use efficiency of the alpine grassland in Tibetan Plateau. J. Geophys. Res.: Atmospheres 127, e2022JD036919. https://doi.org/10.1029/2022jd036919.

Ma, N., Zhang, Y., 2022b. Increasing Tibetan Plateau terrestrial evapotranspiration primarily driven by precipitation. Agric. For. Meteorol. 317, 108887 https://doi.org/10.1016/j.agrformet.2022.108887.

Ma, N., Zhang, Y., Guo, Y., Gao, H., Zhang, H., Wang, Y., 2015a. Environmental and biophysical controls on the evapotranspiration over the highest alpine steppe. J. Hydrol. 529, 980–992. https://doi.org/10.1016/j.jhydrol.2015.09.013.

Ma, N., Zhang, Y., Xu, C.-Y., Szilagyi, J., 2015b. Modeling actual evapotranspiration with routine meteorological variables in the data-scarce region of the Tibetan Plateau: comparisons and implications. J. Geophys. Res.: Biogeosciences 120, 1638–1657. https://doi.org/10.1002/2015jg003006.

Ma, N., Niu, G.-Y., Xia, Y., Cai, X., Zhang, Y., Ma, Y., Fang, Y., 2017. A systematic evaluation of Noah-MP in simulating land-atmosphere energy, water, and carbon exchanges over the continental United States. J. Geophys. Res.: Atmospheres 122, 12245–12268. https://doi.org/10.1002/2017JD027597.

Ma, N., Szilagyi, J., Zhang, Y., 2021. Calibration-free complementary relationship estimates terrestrial evapotranspiration globally. Water Resour. Res. 57, e2021WR029691 https://doi.org/10.1029/2021wr029691.

Ma, Y., Yao, T., Zhong, L., Wang, B., Xu, X., Hu, Z., Ma, W., Sun, F., Han, C., Li, M., Chen, X., Wang, J., Li, Y., Gu, L., Xie, Z., Liu, L., Sun, G., Wang, S., Zhou, D., Zuo, H., Xu, C., Liu, X., Wang, Y., Wang, Z., 2023. Comprehensive study of energy and water exchange over the Tibetan Plateau: a review and perspective: from GAME/Tibet and CAMP/Tibet to TORP, TPEORP, and TPEITORP. Earth-Sci. Rev. 237 https://doi.org/10.1016/j.earscirev.2023.104312.

Miehe, G., Miehe, S., Bach, K., Nölling, J., Hanspach, J., Reudenbach, C., Kaiser, K., Wesche, K., Mosbrugger, V., Yang, Y.P., Ma, Y.M., 2011. Plant communities of central Tibetan pastures in the Alpine Steppe/Kobresia pygmaea ecotone. J. Arid Environ. 75, 711–723. https://doi.org/10.1016/j.jaridenv.2011.03.001.

Niu, G.Y., Fang, Y.H., Chang, L.L., Jin, J., Yuan, H., Zeng, X., 2020. Enhancing the Noah-MP ecosystem response to droughts with an explicit representation of plant water storage supplied by dynamic root water uptake. J. Adv. Model. Earth Syst. 12 https://doi.org/10.1029/2020ms002062.

Niu, G.-Y., Yang, Z.-L., 2007. An observation-based formulation of snow cover fraction and its evaluation over large North American river basins. J. Geophys. Res. 112 https://doi.org/10.1029/2007jd008674.

Niu, G.-Y., Zeng, X., 2012. Earth System Model, Modeling the land component of. In: Rasch, P.J. (Ed.), Climate Change Modeling Methodology: Selected Entries from the Encyclopedia of Sustainability Science and Technology. Springer, New York, pp. 139–168.

Niu, G.-Y., Yang, Z.-L., Mitchell, K.E., Chen, F., Ek, M.B., Barlage, M., Kumar, A., Manning, K., Niyogi, D., Rosero, E., Tewari, M., Xia, Y., 2011. The community Noah land surface model with multiparameterization options (Noah-MP): 1. model description and evaluation with local-scale measurements. J. Geophys. Res. 116 https://doi.org/10.1029/2010jd015139.

Pitman, A.J., 2003. The evolution of, and revolution in, land surface schemes designed for climate models. Int. J. Climatol. 23, 479–510. https://doi.org/10.1002/joc.893.

Sellers, P.J., Dickinson, R.E., Randall, D.A., Betts, A.K., Hall, F.G., Berry, J.A., Collatz, G.J., Denning, A.S., Mooney, H.A., Nobre, C.A., Sato, N., Field, C.B., Henderson-Sellers, A., 1997. Modeling the exchanges of energy, water, and carbon between continents and the atmosphere. Science 275, 502–509. https://doi.org/10.1126/science.275.5299.502.

Shen, M., Piao, S., Cong, N., Zhang, G., Jassens, I.A., 2015. Precipitation impacts on vegetation spring phenology on the Tibetan Plateau. Glob. Chang Biol. 21, 3647–3656. https://doi.org/10.1111/gcb.12961.

Sun, S., Zheng, D., Liu, S., Xu, Z., Xu, T., Zheng, H., Yang, X., 2022. Assessment and improvement of Noah-MP for simulating water and heat exchange over alpine grassland in growing season. Sci. China Earth Sci. 65, 536–552. https://doi.org/10.1360/SSTe-2021-0047.

Wang, P., Niu, G.-Y., Fang, Y.-H., Wu, R.-J., Yu, J.-J., Yuan, G.-F., Pozdniakov, S.P., Scott, R.L., 2018. Implementing dynamic root optimization in Noah-MP for simulating phreatophytic root water uptake. Water Resouces Res. 54, 1560–1575. https://doi.org/10.1002/2017WR021061.

Wang, S., Ma, Y., Liu, Y., 2022b. Simulation of sensible and latent heat fluxes on the Tibetan Plateau from 1981 to 2018. Atmos. Res. 271 https://doi.org/10.1016/j.atmosres.2022.106129.

Wang, T., Wang, P., Wu, Z., Yu, J., Pozdniakov, S.P., Guan, X., Wang, H., Xu, H., Yan, D., 2022a. Modeling revealed the effect of root dynamics on the water adaptability of phreatophytes. Agric. For. Meteorol. 320 https://doi.org/10.1016/j.agrformet.2022.108959.

Warrach-Sagi, K., Ingwersen, J., Schwitalla, T., Troost, C., Aurbacher, J., Jach, L., Berger, T., Streck, T., Wulfmeyer, V., 2022. Noah-MP With the Generic Crop Growth Model Gecros in the WRF Model: effects of Dynamic Crop Growth on Land-Atmosphere Interaction. J. Geophys. Res.: Atmospheres 127, e2022JD036518. https://doi.org/10.1029/2022jd036518.

Wu, G., Duan, A., Liu, Y., Mao, J., Ren, R., Bao, Q., He, B., Liu, B., Hu, W., 2015. Tibetan Plateau climate dynamics: recent research progress and outlook. Natl. Sci. Rev. 2, 100–116. https://doi.org/10.1093/nsr/nwu045.

Xie, Y., Huang, J., Wu, G., Liu, Y., Dong, W., Lu, M., He, B., Su, Z., Bao, Q., Zhao, Q., Liu, Y., 2023. Oceanic repeaters boost the global climatic impact of the Tibetan Plateau. Sci. Bull. https://doi.org/10.1016/j.scib.2023.07.019.

Yang, K., Chen, Y., Qin, J., 2009a. Some practical notes on the land surface modeling in the Tibetan Plateau. Hydrol. Earth Syst. Sci. 13, 687–701.

Yang, K., Wu, H., Qin, J., Lin, C., Tang, W., Chen, Y., 2014. Recent climate changes over the Tibetan Plateau and their impacts on energy and water cycle: a review. Glob. Planet. Change 112, 79–91. https://doi.org/10.1016/j.gloplacha.2013.12.001.

Yang, Y., Fang, J., Ji, C., Han, W., 2009b. Above- and belowground biomass allocation in Tibetan grasslands. J. Veg. Sci. 20, 177–184.

Yao, T., Xue, Y., Chen, D., Chen, F., Thompson, L., Cui, P., Koike, T., Lau, W.K.M., Lettenmaier, D., Mosbrugger, V., Zhang, R., Xu, B., Dozier, J., Gillespie, T., Gu, Y., Kang, S., Piao, S., Sugimoto, S., Ueno, K., Wang, L., Wang, W., Zhang, F., Sheng, Y., Guo, W., Ailikun, Yang, X., Ma, Y., Shen, S.S.P., Su, Z., Chen, F., Liang, S., Liu, Y., Singh, V.P., Yang, K., Yang, D., Zhao, X., Qian, Y., Zhang, Y., Li, Q., 2019. Recent Third Pole's rapid warming accompanies cryospheric melt and water cycle intensification and interactions between monsoon and environment: multidisciplinary approach with observations, modeling, and analysis. Bull. Am. Meteorol. Soc. 100, 423–444. https://doi.org/10.1175/bams-d-17-0057.1.

Zhang, Z., Arnault, J., Laux, P., Ma, N., Wei, J., Shang, S., Kunstmann, H., 2022. Convection-permitting fully coupled WRF-Hydro ensemble simulations in high mountain environment: impact of boundary layer- and lateral flow parameterizations on land–atmosphere interactions. Clim. Dynam. 59, 1355–1376. https://doi.org/10.1007/s00382-021-06044-9.

Zhang, G., Chen, F., Gan, Y., 2016. Assessing uncertainties in the Noah-MP ensemble simulations of a cropland site during the Tibet Joint International Cooperation program field campaign. J. Geophys. Res.: Atmospheres 121, 9576–9596. https://doi.org/10.1002/2016jd024928.

Zhang, J., Wang, J.T., Chen, W., Li, B., Zhao, K., 1988. Vegetation of Xizang (Tibet). Science Press.

Zhang, Z., Wang, K., 2020. Stilling and recovery of the surface wind speed based on observation, reanalysis, and geostrophic wind theory over China from 1960 to 2017. J. Clim. 33, 3989–4008. https://doi.org/10.1175/jcli-d-19-0281.1.

Zheng, D., van der Velde, R., Su, Z., Booij, M.J., Hoekstra, A.Y., Wen, J., 2014. Assessment of Roughness Length Schemes Implemented within the Noah Land Surface Model for High-Altitude Regions. J. Hydrometeorol. 15, 921–937. https://doi.org/10.1175/jhm-d-13-0102.1.

Zheng, D., van der Velde, R., Su, Z., Wang, X., Wen, J., Booij, M.J., Hoekstra, A.Y., Chen, Y., 2015a. Augmentations to the Noah Model Physics for Application to the Yellow River Source Area. Part I: soil Water Flow. J. Hydrometeorol. 16, 2659–2676. https://doi.org/10.1175/jhm-d-14-0198.1.

Zheng, D., van der Velde, R., Su, Z., Wang, X., Wen, J., Booij, M.J., Hoekstra, A.Y., Chen, Y., 2015b. Augmentations to the Noah Model Physics for Application to the Yellow River Source Area. Part II: turbulent Heat Fluxes and Soil Heat Transport. J. Hydrometeorol. 16, 2677–2694. https://doi.org/10.1175/jhm-d-14-0199.1.

Zheng, D., Van der Velde, R., Su, Z., Wen, J., Booij, M.J., Hoekstra, A.Y., Wang, X., 2015c. Under-canopy turbulence and root water uptake of a Tibetan meadow ecosystem modeled by Noah-MP. Water Resour. Res. 51, 5735–5755. https://doi.org/10.1002/2015WR017115.

Zhu, G., Su, Y., Li, X., Zhang, K., Li, C., 2013. Estimating actual evapotranspiration from an alpine grassland on Qinghai-Tibetan plateau using a two-source model and parameter uncertainty analysis by Bayesian approach. J. Hydrol. 476, 42–51. https://doi.org/10.1016/j.jhydrol.2012.10.006.